Electronic Supplementary Material (ESI) for Energy & Environmental Science.

Supplementary information

Realizing thermoelectric conversion efficiency of 12% in Bismuth Telluride/Skutterudite segmented modules through full-parameter optimization and energy-loss minimized integration

Qihao Zhang,[ab] Jincheng Liao,[a] Yunshan Tang,[a] Ming Gu,[a] Chen Ming,[a] Pengfei Qiu,[a] Shengqiang Bai,*[a] Xun Shi,[a] Ctirad Uher*[c] and Lidong Chen*[ad]

[a] State Key Laboratory of High Performance Ceramics and Superfine Microstructure, Shanghai Institute of Ceramics, Chinese Academy of Sciences, Shanghai, 200050, China. E-mail: bsq@mail.sic.ac.cn, cld@mail.sic.ac.cn

[b] University of Chinese Academy of Sciences, 19 Yuquan Road, Beijing, 100049, China

[c] Department of Physics, University of Michigan, Ann Arbor, MI 48109, USA. E-mail: cuher@umich.edu

[d] CAS Key Laboratory of Materials for Energy Conversion, Shanghai Institute of Ceramics, Chinese Academy of Science, Shanghai 200050, China

This supplement contains

Supplementary Figures 1-17

Supplementary Tables 1-2

Supplementary Methods

Supplementary References

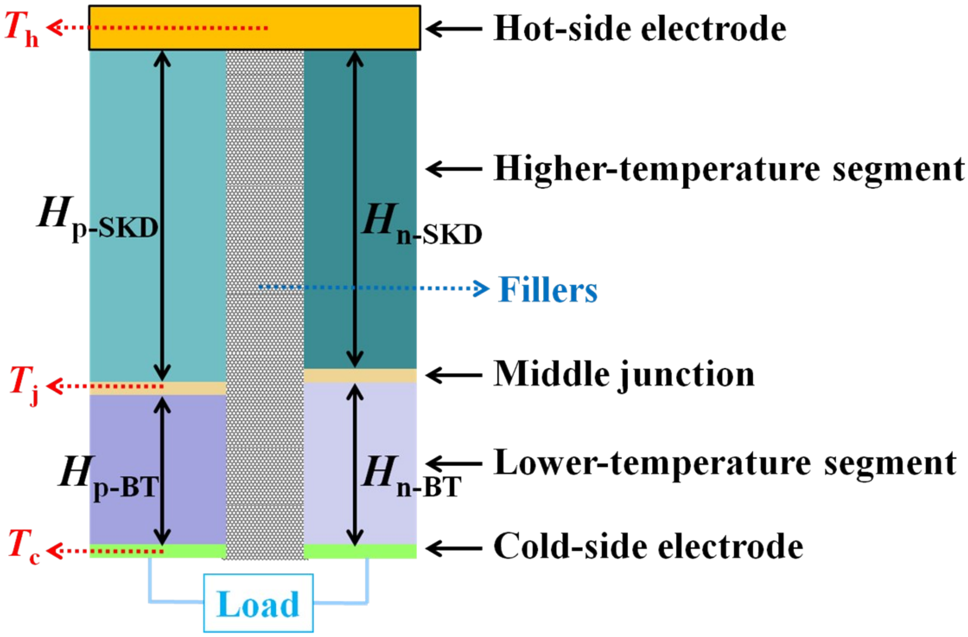

Supplementary Figure 1| A schematic diagram of a segmented TE unicouple.

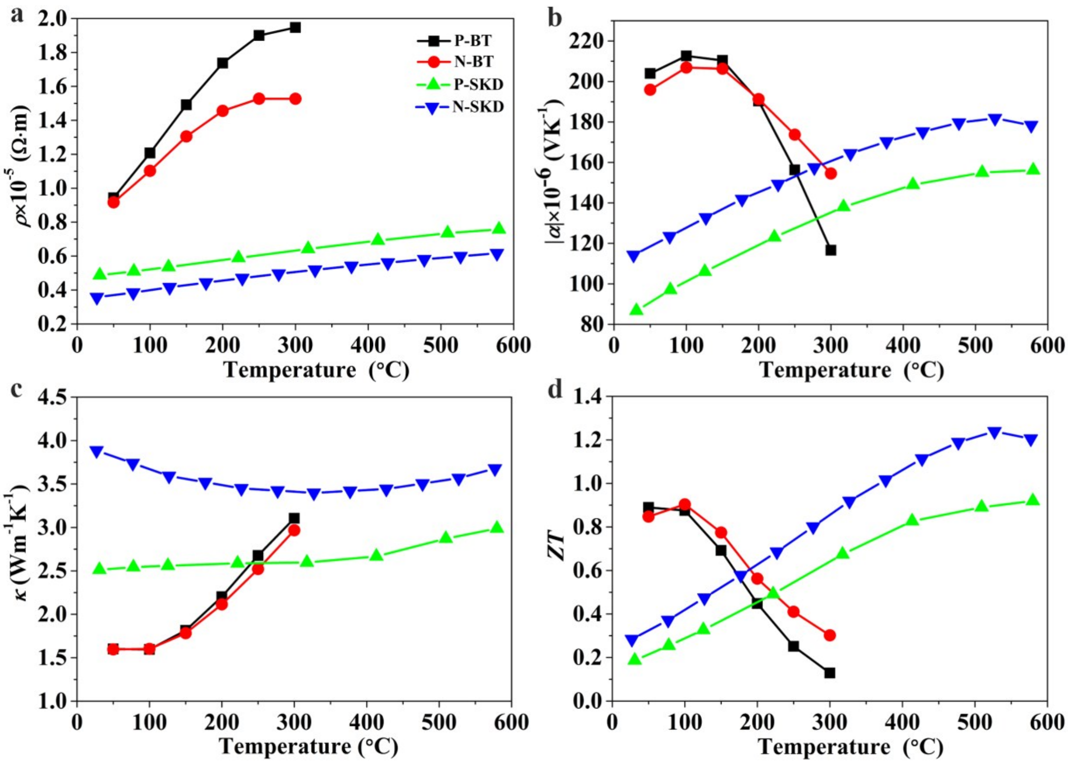

Supplementary Figure 2| Temperature dependence of (a) the electrical resistivity (ρ), (b) the absolute Seebeck coefficient ($|\alpha|$), (c) the thermal conductivity (κ) and (d) the dimensionless figure of merit *ZT* for bismuth telluride (p-$Bi_{0.4}Sb_{1.6}Te_3$ and n-$Bi_2Te_{2.5}Se_{0.5}$) and skutterudite (p-$CeFe_{3.85}Mn_{0.15}Sb_{12}$ and n-$Yb_{0.3}Co_4Sb_{12}$). The TE performances were characterized by commercial equipments (ZEM-3 and the Laser Flash method).

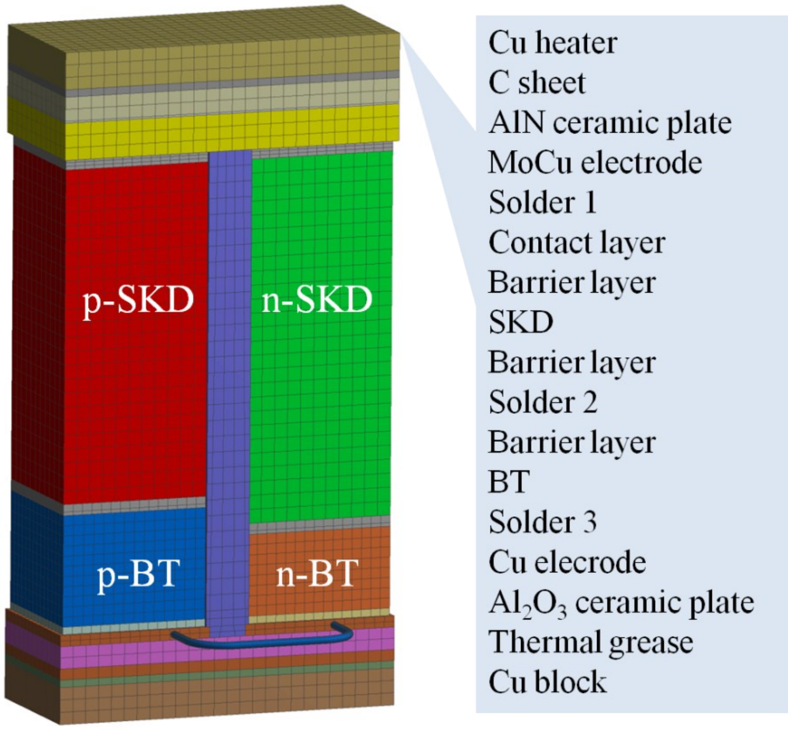

Supplementary Figure 3| The 3D finite element model of the BT/SKD segmented power generation unicouple after removing the outer insulating material. The text on the right details the components from the top to the bottom of the BT/SKD segmented unicouple used in this work.

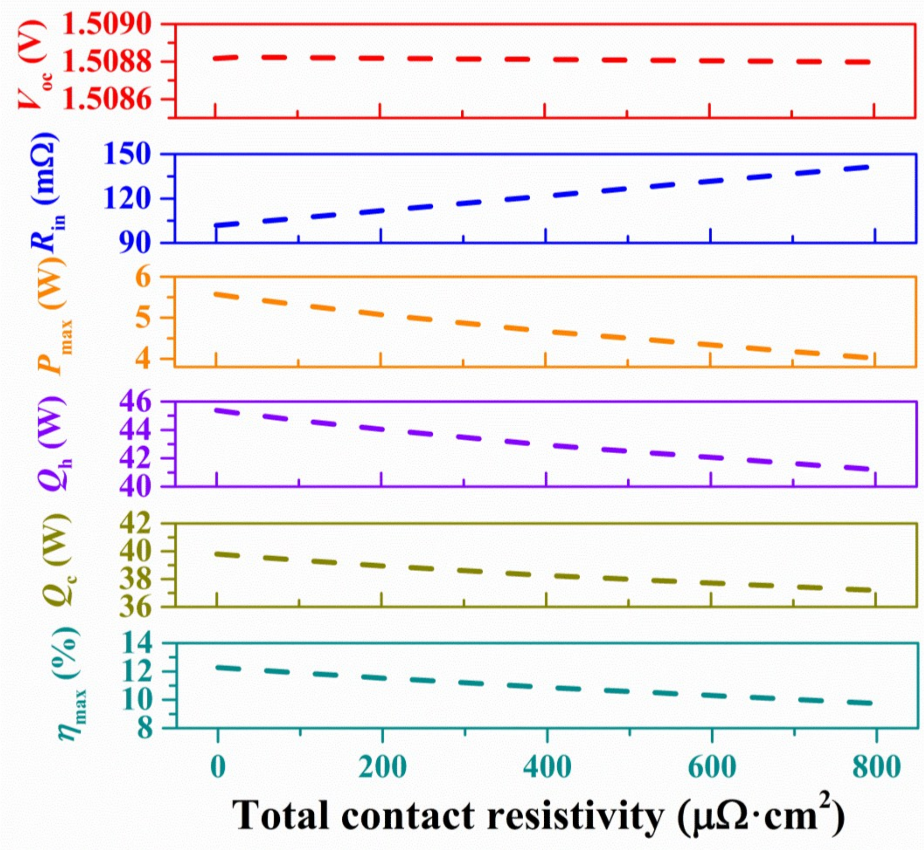

Supplementary Figure 4| The effect of the total contact resistivity of the segmented unicouple on the open-circuit voltage (V_{oc}), module internal resistance (R_{in}), maximum output power (P_{max}), absorbed heat (Q_h) and released heat (Q_c). The simulations was performed under T_h=578 °C and T_c=38 °C. V_{oc} remains unchanged while R_{in} gradually increases with the increasing total contact resistivity. Although Q_h becomes lower as well, due to the increased Joule heat released on the hot side, η_{max} inevitably falls off as a result of the more significantly reduced output power.

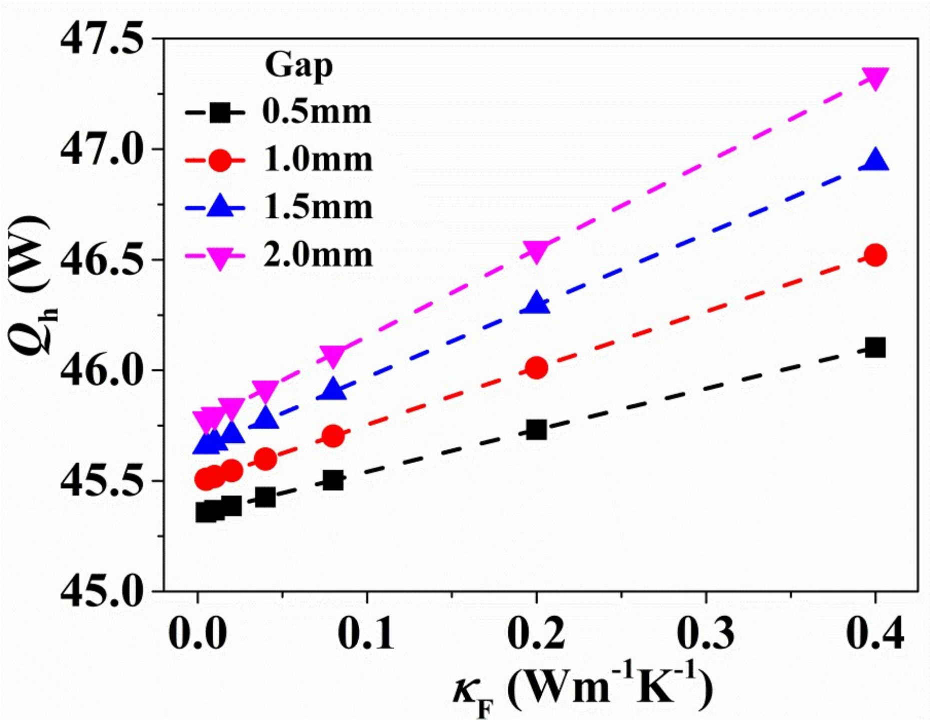

Supplementary Figure 5| The effect of the thermal conductivity of the fillers (κ_F) on the absorbed heat (Q_h) under different gaps between *p*- and *n*-type legs.

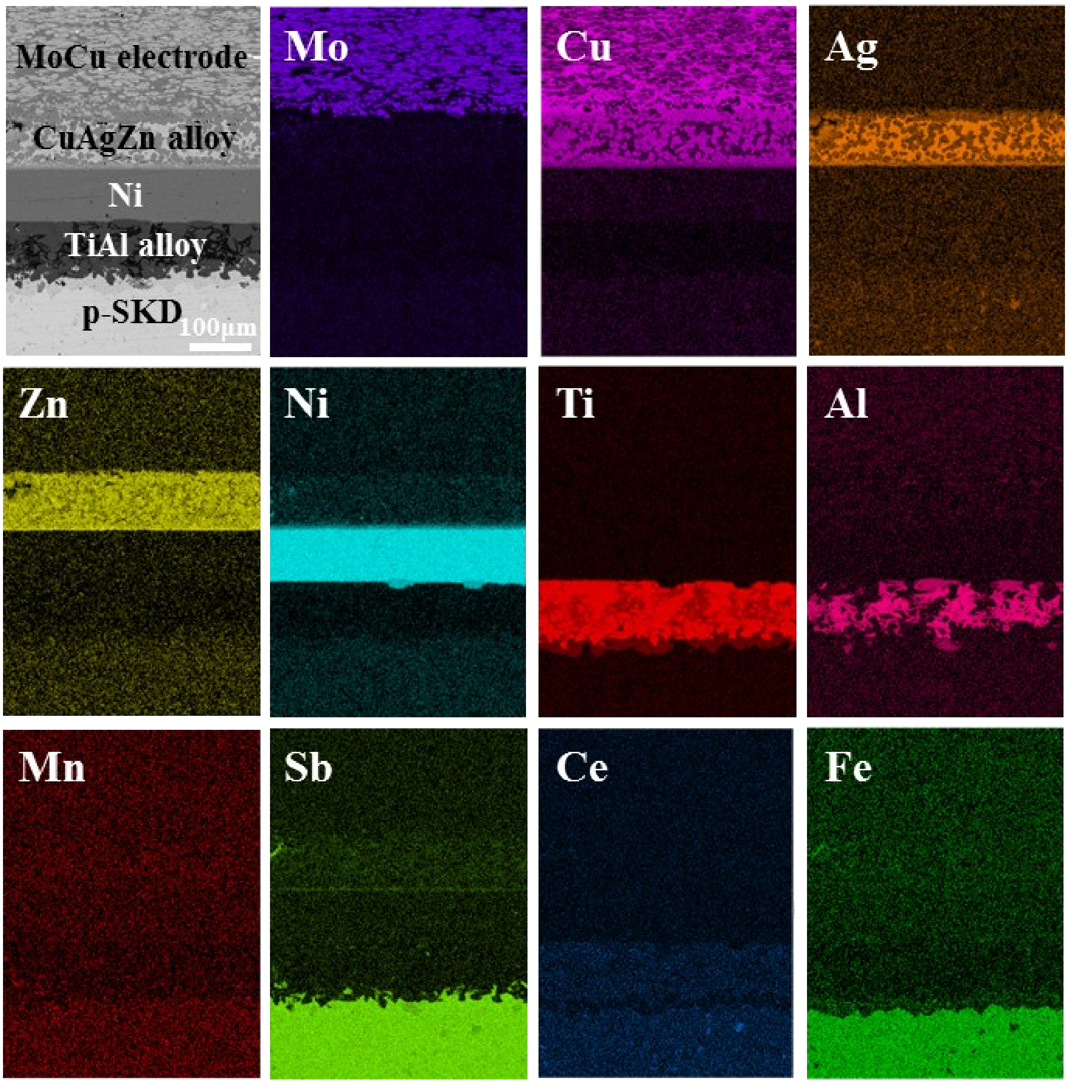

Supplementary Figure 6| SEM image and EDS mapping of the interface between the MoCu electrode and *p*-SKD.

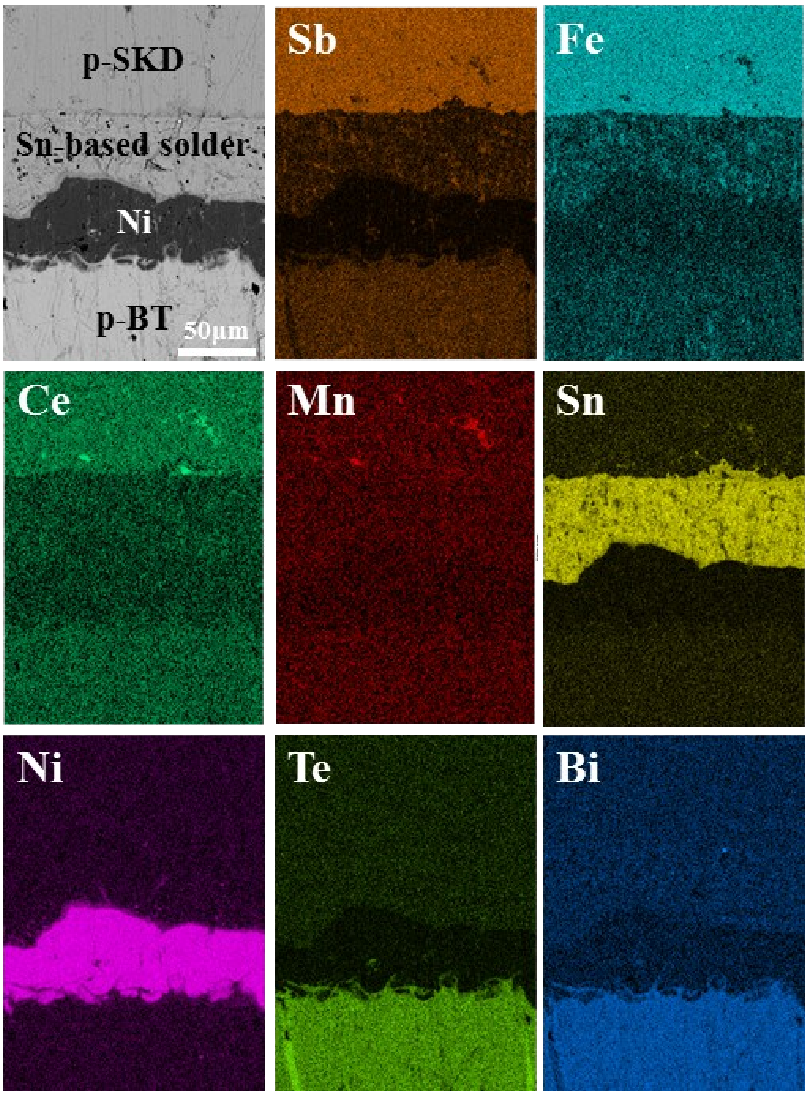

Supplementary Figure 7| SEM image and EDS mapping of the interface between *p*-SKD and *p*-BT.

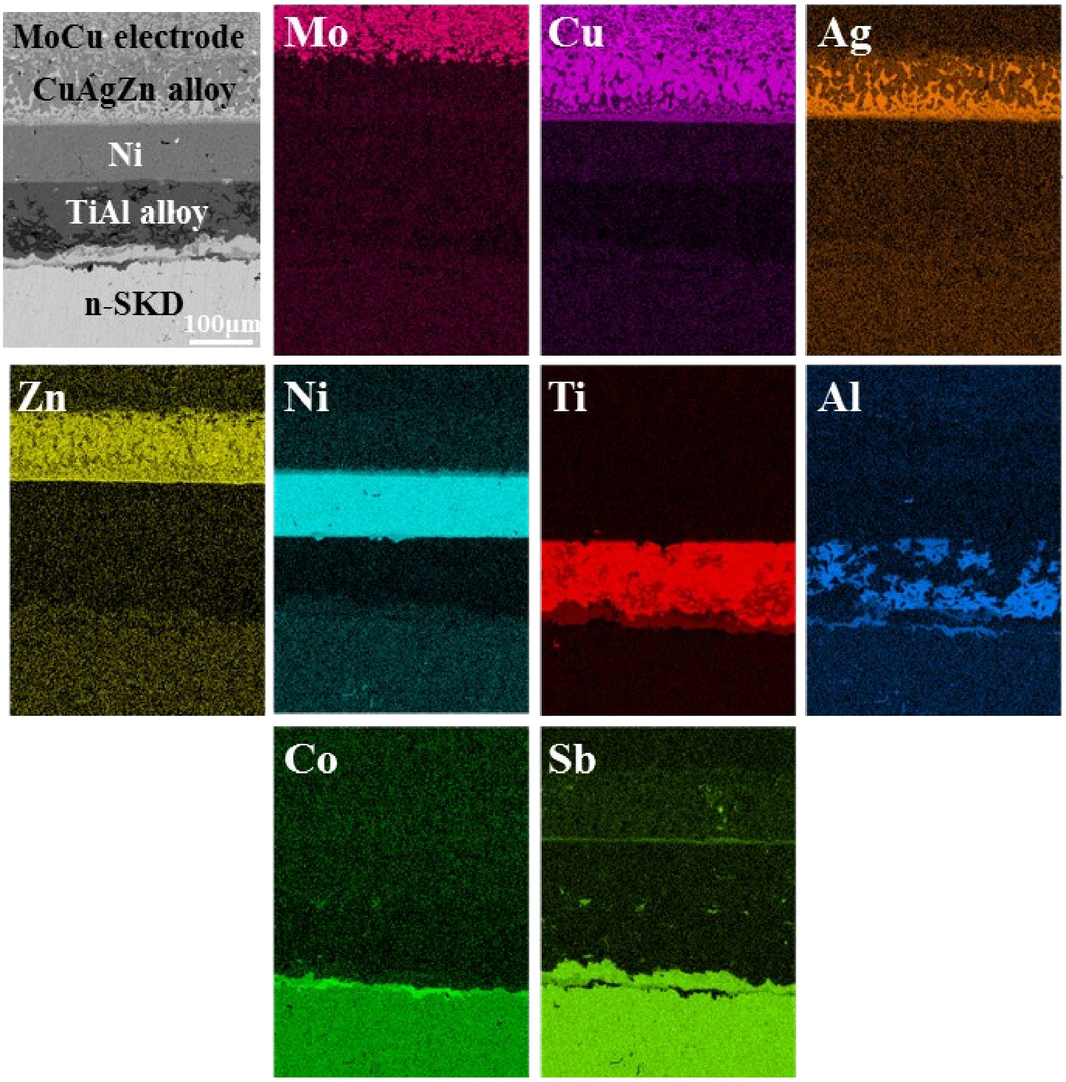

Supplementary Figure 8| SEM image and EDS mapping of the interface between the MoCu electrode and *n*-SKD.

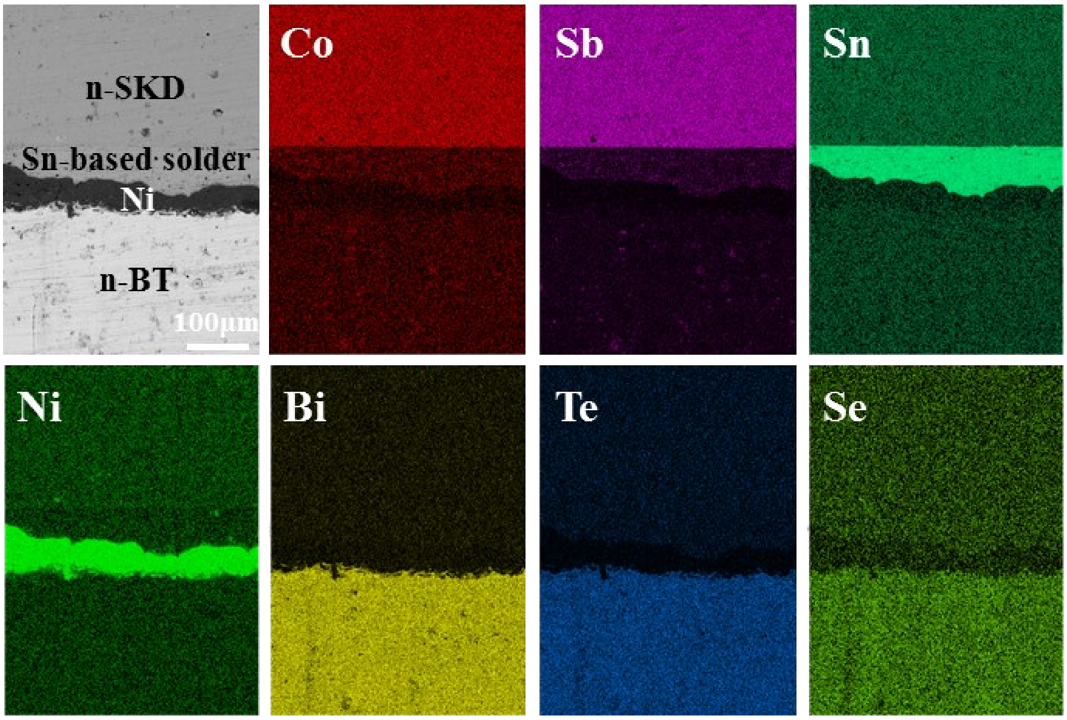

Supplementary Figure 9| SEM image and EDS mapping of the interface between *n*-SKD and *n*-BT.

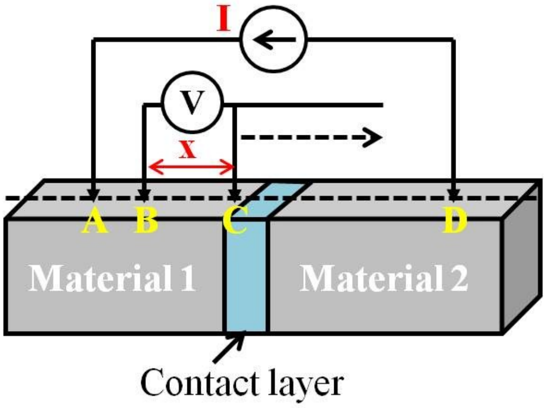

Supplementary Figure 10| Schematic diagram of a measurement of the electrical contact resistance by a four-probe method.

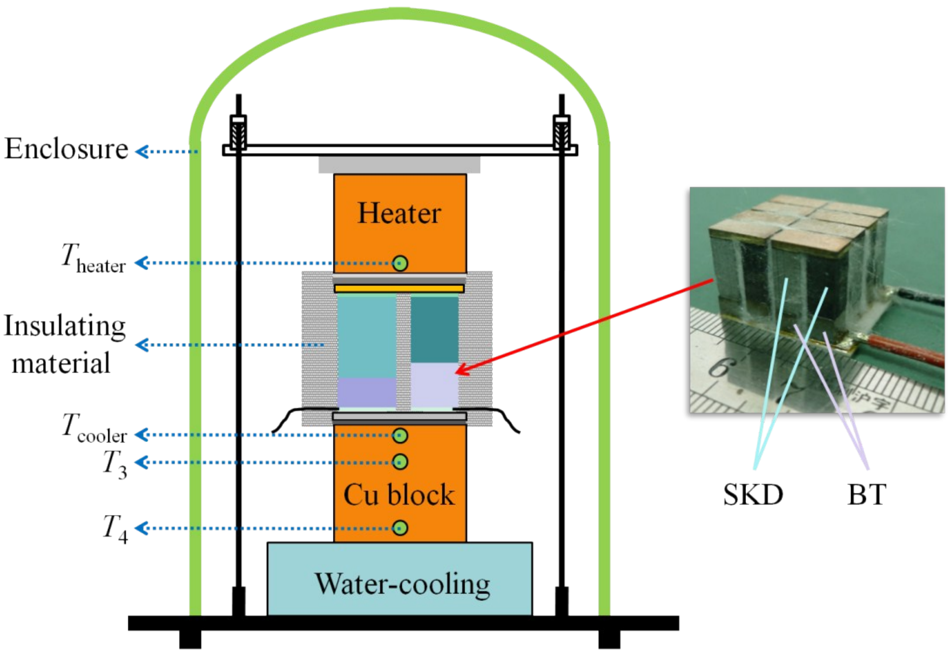

Supplementary Figure 11| Schematic diagram of the testing system.

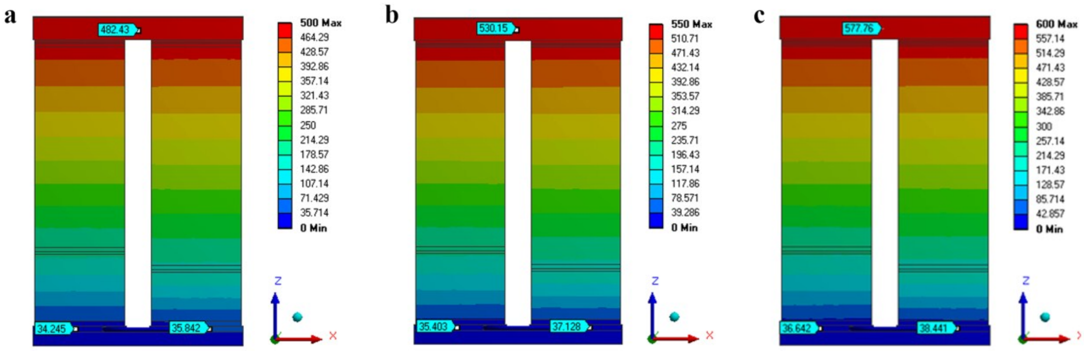

Supplementary Figure 12| Temperature profiles determined from the numerical simulation at different operating temperatures taking fully into account the measured interfacial heat transfer coefficient. **a,** T_{heater} =500 °C and T_{cooler} =25 °C. **b,** T_{heater} =550 °C and T_{cooler} =25 °C. **c,** T_{heater} =600 °C and T_{cooler} =25 °C. The insulating material surrounding the TE legs has been removed to provide a clear view.

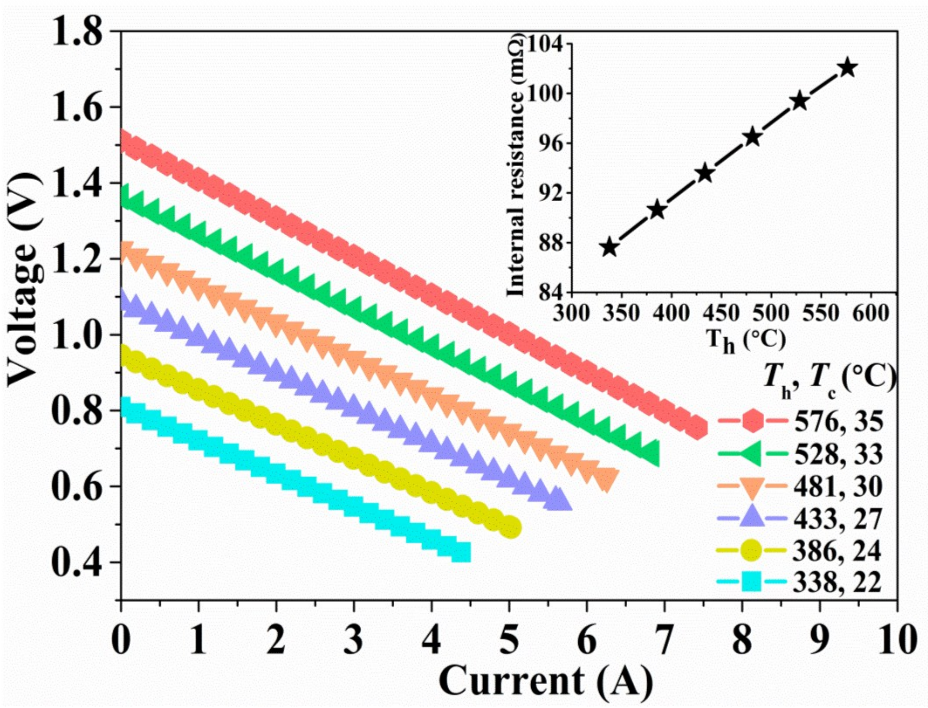

Supplementary Figure 13| Voltage-current curves under different operating temperatures; the inset depicts the module's internal resistance (R_{in}) as a function of T_h. The open-circuit voltage (V_{oc}) increases from 0.81 to 1.51 V as the T_h rises from 338 to 576 °C, corresponding to the increased Seebeck coefficient (Supplementary Fig. 2b) and ΔT. Synchronously, R_{in} rises from 87.6 to 102.1 mΩ with the increasing temperature, consistent with the increasing electrical resistivity of TE materials at elevated temperatures (Supplementary Fig. 2a).

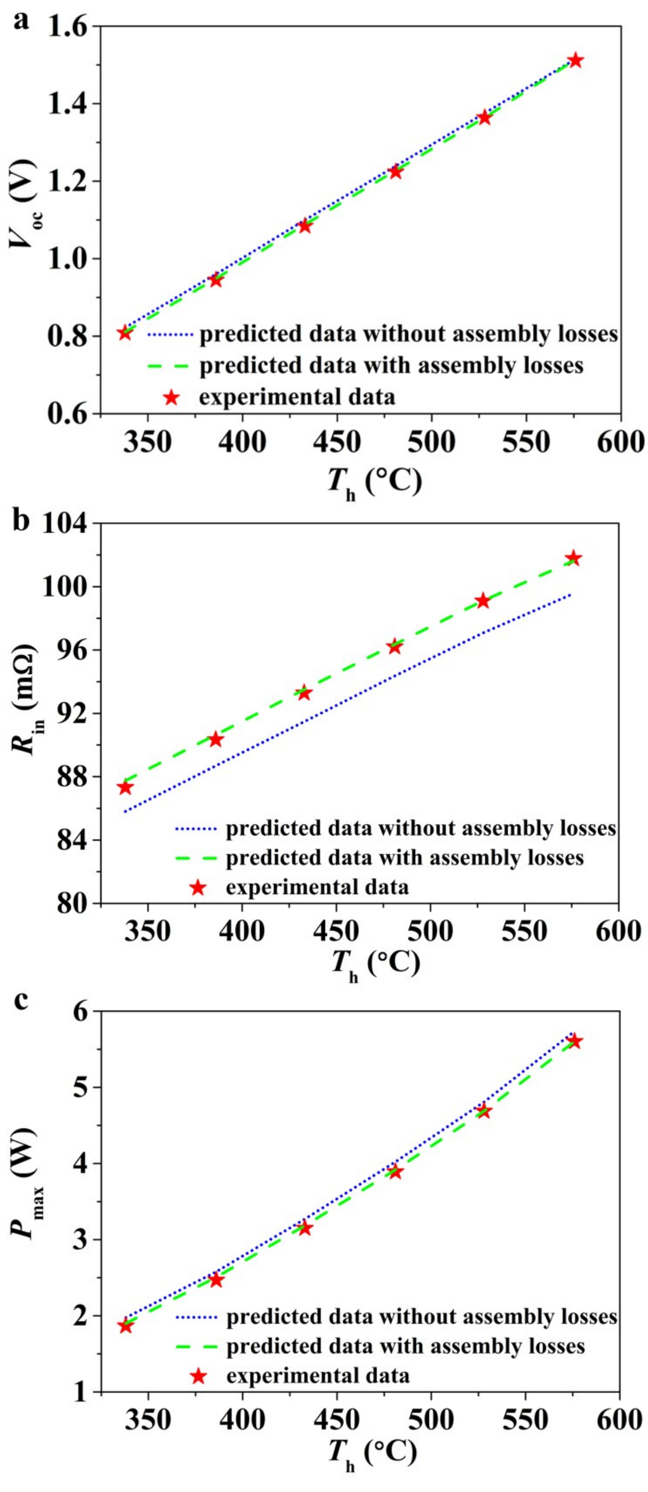

Supplementary Figure 14| Comparison of experimental values with simulations. (a) Open-circuit voltage, (b) module's resistance, and (c) maximum output power as a function of the hot-side electrode temperature under different conditions.

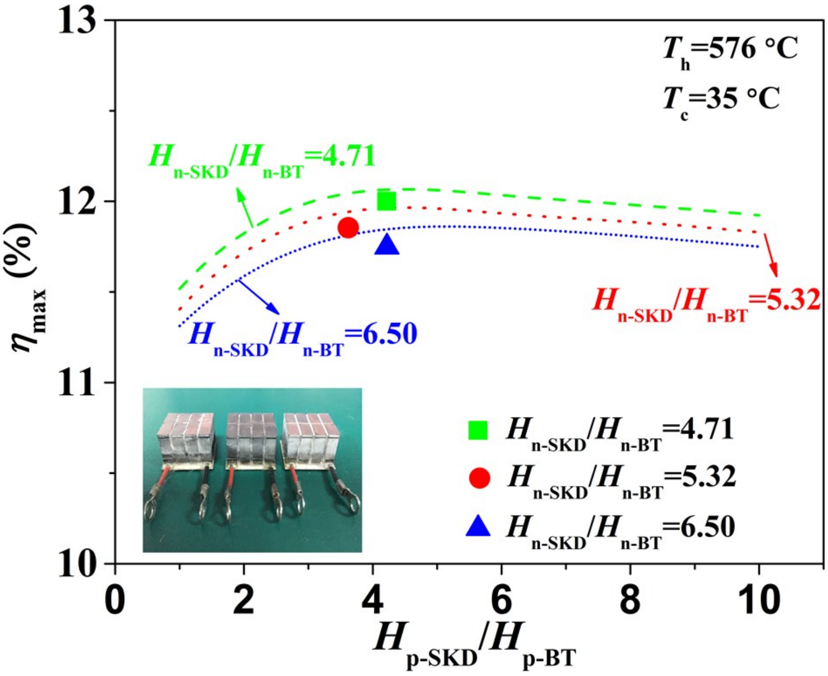

Supplementary Figure 15| The comparison between experimental values (scattered points) and simulation values with assembly losses (dashed curves) for the segmented modules having different height ratio. The inset shows three measured segmented modules. The total height of TE materials of each leg is 12 mm and the cross section is 4.0 mm×4.0 mm. Each module with the overall size of 20 mm×20 mm×14.5 mm possesses eight unicouples.

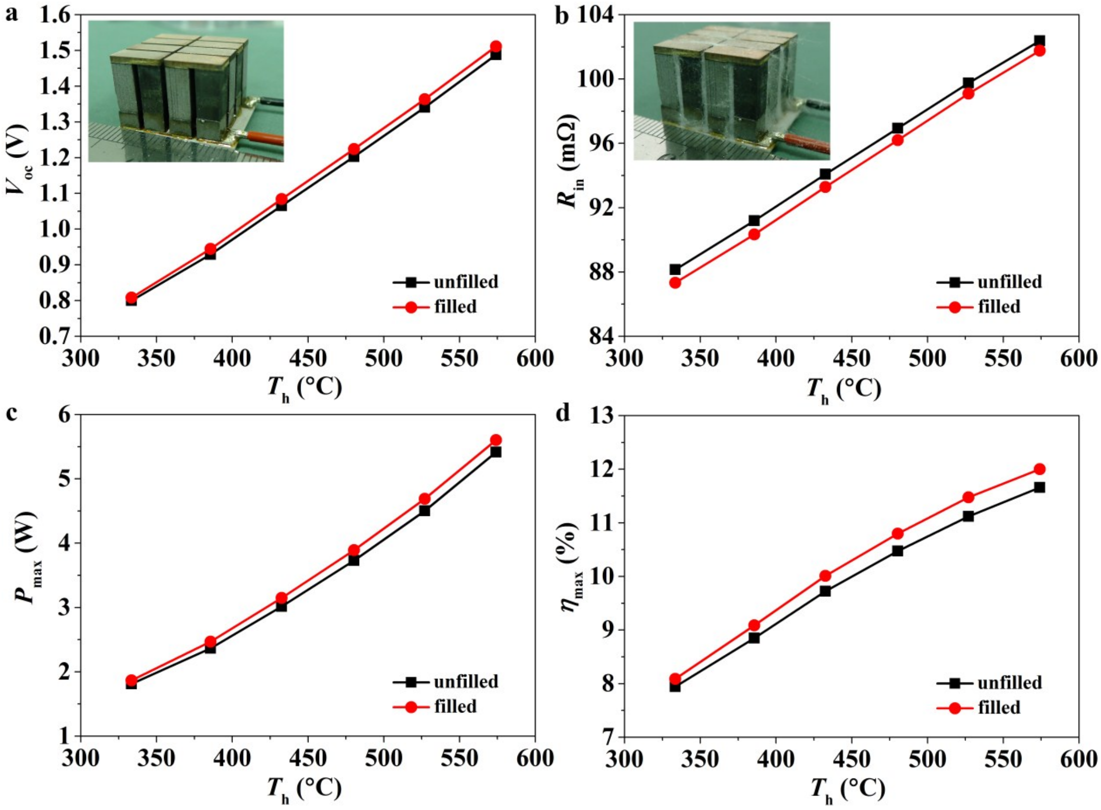

Supplementary Figure 16| Comparison of performances of segmented modules with and without fillers under the same test conditions. a, Open-circuit voltage; the inset shows a segmented module without fillers. **b,** Module's resistance; the inset shows a segmented module with fillers. **c,** Maximum output power. **d,** Maximum conversion efficiency.

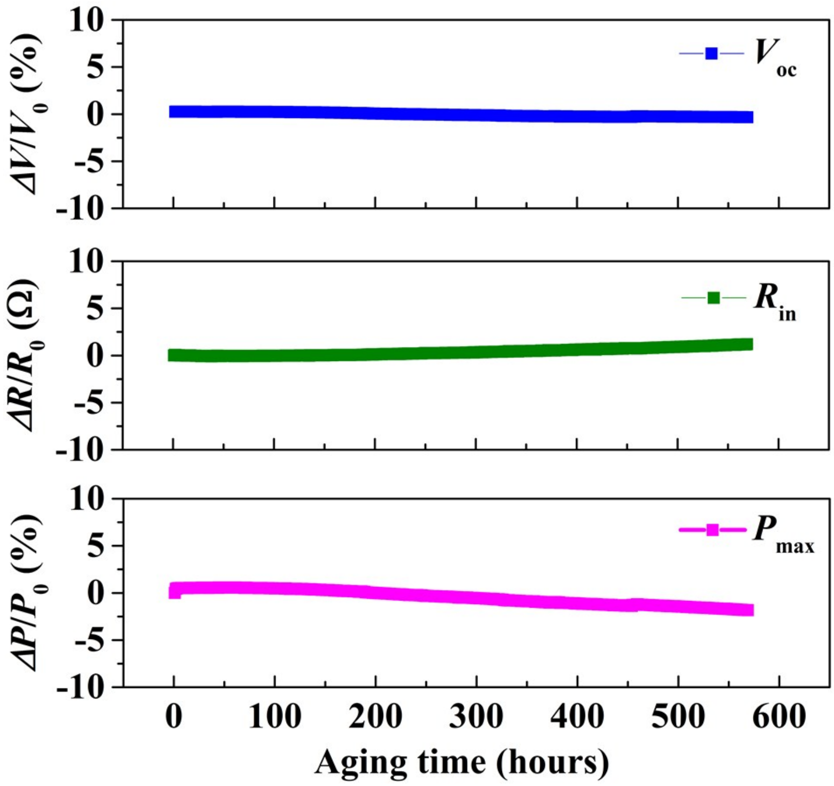

Supplementary Figure 17| The results of aging testing on the BT/SKD segmented module under the constant temperature difference of 520 ℃ with an argon atmosphere. From top to bottom, the results correspond to the percentage change of open-circuit voltage (V_{oc}), module's internal resistance (R_{in}), and maximum power output (P_{max}), respectively.

Supplementary Table 1| Details regarding material's parameters used in the analysis.

	Thermal conductivity ($Wm^{-1}K^{-1}$)	Electrical resistivity (ohmm)	Description
AlN	200	--	insulating ceramic plate
$Mo_{50}Cu_{50}$	250	2.67×10^{-8}	hot-side electrode
Ag-Cu-Zn	401	1.68×10^{-8}	hot-side brazing solder
Ti-Al	21.9	5.26×10^{-7}	barrier layer
Ni	90	6.25×10^{-8}	contact layer
SnSb Solder	55	1.14×10^{-7}	cold-side solder
Cu	380-260 (3~150 °C)	1.68×10^{-8}	cold-side electrode and heat-flow meter
Al_2O_3	30.3-9.1 (100~600 °C)	--	insulating ceramic plate
Thermal glue	1.7	--	heat conduction

Supplementary Table 2| Details regarding the dimension of the BT/SKD segmented module; the unit of each number is mm.

n-type leg		*p*-type leg		gap
BT	SKD	BT	SKD	1.0
4.0×4.0×2.1	4.0×4.0×9.9	4.0×4.0×2.3	4.0×4.0×9.7	

Supplementary Methods

S1. Electrical contact resistance measurement

Contact resistance measurements were performed through a custom-built test bench based on a four-probe method. As shown in Supplementary Fig. 10, when the current is applied between points A and D, the voltage between points B and C can be determined. The probe at point B is fixed, while the probe at point C moves at preset steps from one material to another. From the applied current (I_{AD}) and the measured voltage (V_{BC}), the resistance between B and C is calculated by $R_{BC}=V_{BC}/I_{AD}$. When the probe C moves across the contact layer, the following expression can be derived:

$$R_{BC} = R_1 + R_c + R_2 \tag{1}$$

where R_1, R_c and R_2 are resistances of material 1, contact layer and material 2, respectively. R_c was obtained from the intercept of the resistances *versus* position plot. The contact electrical resistivity (ρ_c) then follows from

$$\rho_c = R_c \cdot S \tag{2}$$

where S is the cross-sectional area of the element. The measurements were performed at room temperature.

S2. Thermal contact resistance measurement

Thermal contact resistances are inevitably present between the TE module and the external heat/cold source even when clamped under pressure. This leads to an additional temperature drop that reduces the effective temperature difference across the TE materials. However, it is quite difficult to obtain accurate temperatures of the two sides of the TE module due to the complexity of the TE device. Researchers have tried to drill a hole on the electrode or on the ceramic plate to assess the temperatures using thermocouples.[1-3] However, thermocouples require good physical contact, which could destroy the structure of the TE module. Some papers also reported on the use of infrared imaging to record the temperature.[4,5] However, the generally low spatial resolution triggers a new problem, especially for large temperature differences in excess of 500 °C.

In this work, we have tried to obtain the thermal contact resistances using a home-made testing system (Fig. 4a). The contacts were maintained using four compression springs, with which one can adjust the pressure over the TE module. The TE module was merely used to establish the temperature difference and thus was kept in an open-circuit state. Referring to Fig. 4a, the thermocouples were used to measure temperatures of the heater, two extra copper plates 1 and 2, and a cooling Cu block so as not to affect the integrity of the device. All materials under the test have the same cross-sectional area. Excellent insulating materials were used to enclose the TE module to ensure a one-dimensional nature of heat transfer as much as possible. The measurement was conducted inside a water cooled chamber filled with argon. According to the schematic diagram in Fig. 4a, the following relationship can be derived:

$$\frac{T_{heater} - T_1}{\Psi_h} = \frac{T_2 - T_{cooler}}{\Psi_c} = \frac{T_3 - T_4}{\Psi_{Cu}}$$

(3)

where Ψ_{h} is the thermal resistance between the heater and Copper 1, Ψ_{c} is the thermal resistance between Copper 2 and the Cu block, and Ψ_{Cu} is the thermal resistance of the water-cooled Cu block. Ψ_{h} and Ψ_{c} can be obtained, provided that the thermal conductivity of the Cu block was measured in advance. Ψ_{Cu} is calculated from

$$\Psi_{Cu} = \frac{L}{\kappa_{Cu} A_{Cu}} \tag{4}$$

where κ_{Cu} and A_{Cu} are the thermal conductivity and the cross-sectional area of the Cu block, respectively. L is the vertical distance between thermocouples T_3 and T_4 in Fig. 4a. Ultimately, the interfacial heat transfer coefficient of the hot-side contact (h_{h}) between the heater and Copper 1 and the heat transfer coefficient of the cold-side contact (h_{c}) between Copper 2 and the Cu block are obtained by

$$h_h = \frac{1}{\Psi_h A_{Cu}} \tag{5}$$

$$h_c = \frac{1}{\Psi_c A_{Cu}} \tag{6}$$

S3. The preparation process of n-type SKD

The polycrystalline ingot with nominal composition of $Yb_{0.3}Co_4Sb_{12}$ was synthesized from high pure elements, Yb (99.95%), Co (99.95%), and Sb (99.99%) by melting quenching annealing method. The raw elements were loaded into a quartz tube with carbon pre-deposited on the inner wall, and sealed under a pressure of 0.1 Pa. All the above procedures were carried out in a glovebox filled with high-purity Ar (O_2 < 0.1 ppm, H_2O < 5 ppm). The elements were then melted at 1353 K for 24 h, quenched into water bath and annealed at 973 K for 120 h. The obtained ingot was ground into fine powder and passed through the 200 mesh screen for further use.

S4. The preparation process of p-type SKD

The polycrystalline ingot with nominal composition of $CeFe_{3.85}Mn_{0.15}Sb_{12}$ was synthesized from high pure elements, Ce (99.9%), Fe (99.99%), Mn (99.95%), and Sb (99.99%), by melting quenching annealing method. The raw elements were sealed in evacuated quartz ampoules coated with carbon in a glovebox and heated slowly up to 1350 K for 10 h, then quenched into water bath, and annealed at 973 K for 168 h. The obtained ingot was ground into fine powder and passed through the 200 mesh screen for further use.

References

1. Fleurial, J. P., Johnson, K., Mondt, J. & Sakamoto, J. Development of segmented thermoelectric multicouple converter technology. In *Aerospace Conference* (IEEE, 2006).
2. Takazawa, H., Obara, H., Okada, Y. & Kobayashi, K. Efficiency measurement of thermoelectric modules operating in the temperature difference of up to 550 K. In *2006, Twenty-fifth International Conference on Thermoelectrics-ICT* 189-192 (IEEE, 2006).
3. El-Genk, M. S., Saber, H. H., Caillat, T. & Sakamoto, J. Tests results and performance comparisons of coated and un-coated skutterudite based segmented

unicouples. *Energy Convers. Manage.* **47,** 174-200 (2006).

4. D'Angelo, J. *et al.* Electrical, thermal, and mechanical characterization of novel segmented-leg thermoelectric modules. *J. Electron. Mater.* **40,** 2051-2062 (2011).
5. Barako, M. T., Park, W., Marconnet, A. M., Asheghi, M. & Goodson, K. E. Thermal cycling, mechanical degradation, and the effective figure of merit of a thermoelectric module. *J. Electron. Mater.* **42,** 372-381 (2013).